

---

# Nearness of Neighbors Attention for Regression in Supervised Fine-Tuning

---

**Aviad Susman**

Department of Population Health  
Icahn School of Medicine at Mount Sinai  
New York, NY 10029  
aviad.susman@mssm.edu

**Mayte Suárez-Fariñas**

Department of Population Health  
Icahn School of Medicine at Mount Sinai  
New York, NY 10029  
mayte.suarezfarinas@mssm.edu

**Joseph T Colonel**

Windreich Department of AI and Human Health  
Icahn School of Medicine at Mount Sinai  
New York, NY 10029  
joseph.colonel@mssm.edu

## Abstract

It is common in supervised machine learning to combine the feature extraction capabilities of neural networks with the predictive power of traditional algorithms, such as k-nearest neighbors (k-NN) or support vector machines. This procedure involves performing supervised fine-tuning (SFT) on a domain-appropriate feature extractor, followed by training a traditional predictor on the resulting SFT embeddings. When used in this manner, traditional predictors often deliver increased performance over the SFT model itself, despite the fine-tuned feature extractor yielding embeddings specifically optimized for prediction by the neural network’s final dense layer. This suggests that directly incorporating traditional algorithms into SFT as prediction layers may further improve performance. However, many traditional algorithms have not been implemented as neural network layers due to their non-differentiable nature and their unique optimization requirements. As a step towards solving this problem, we introduce the Nearness of Neighbors Attention (NONA) regression layer. NONA uses the mechanics of neural network attention and a novel learned attention-masking scheme to yield a differentiable proxy of the k-NN regression algorithm. Results on multiple unstructured datasets show improved performance over both dense layer prediction and k-NN on SFT embeddings for regression.

## 1 Introduction

Supervised fine-tuning (SFT) has become a primary tool in supervised learning on unstructured data across various domains, including computer vision and natural language processing [1]. The success of SFT arises from its ability to generate powerful and generalizable representations from small- to mid-sized datasets. However, it is common within many application contexts where SFT is leveraged to use the representations generated by large fine-tuned neural networks to train traditional machine learning algorithms for the ultimate prediction task [2–4]. The motivation behind this practice lies in the common observation that traditional predictors often deliver increased performance compared to the predictions of the SFT model itself. The continued success of traditional prediction in this context is particularly noteworthy given that, in SFT, the feature extractor is optimized to embed data specifically for prediction by the neural network model’s final dense layer. While surprising,

this aligns with the well-studied phenomenon that deep-learning-based models fail to outperform traditional predictors in the structured data domain [5].

A natural question motivated by this paradigm is whether the use of a traditional algorithm as a prediction layer directly within SFT might result in improved performance over both the dense prediction layer and the two-step SFT procedure, as the feature extractor would be optimized to embed data in a complementary way to the ultimate downstream predictor. However, many common prediction algorithms are not differentiable and so cannot be incorporated into deep learning systems, including for SFT.

To facilitate the integration of traditional and deep learning methods for prediction, we introduce the Nearness of Neighbors Attention (NONA) regression layer. NONA uses the basic mechanics of a neural network attention block and a novel parameterized masking procedure to yield a differentiable proxy of the k-nearest neighbors (k-NN) regression algorithm. Results on several unstructured datasets across multiple domains and dataset sizes show improved performance over dense layer prediction as well as k-NN prediction on dense layer SFT embeddings.

The contributions of this paper are as follows:

- We define the NONA regression layer using the mechanisms of neural network attention.
- We propose a learned attention-masking scheme, SoftStep, to approximate the neighbor ranking and rejection algorithm of traditional k-NN.
- We present a theoretical analysis demonstrating that NONA paired with mean-square error (MSE) loss implicitly enforces a pair-wise and triplet loss on the embedding space constructed by the feature extractor.
- We illustrate NONA’s superior performance to dense layer regression and dense layer-based two-stage supervised finetuning with k-NN on several datasets.

A GitHub repository containing the full implementation of our methods and all experimentation is available at [github.com/aviadsusman/nona\\_anon](https://github.com/aviadsusman/nona_anon).

## 2 Related Work

**Two-Stage Supervised Finetuning** Neural networks are renowned for their performance in classification and regression tasks on unstructured data [6]. This performance is due in part to the computational structure of neural networks, which can extract salient information from inputs prior to any learning on data [7, 8]. In some applications, pretrained neural networks are treated as feature extractors for traditional machine learning algorithms such as k-NN and support vector machines [9]. In small- to mid-size data regimes, where training a neural network from scratch will lead to poor generalization, supervised finetuning of a pretrained neural network can help improve performance on data domains of interest [10, 11]. This two-stage process - supervised finetuning of a pretrained neural network followed by fitting extracted features from the finetuned model on different classification and regression algorithms - has seen widespread success in various tasks [12–17].

**Neighbor-based models** Neighbor-based models use decision rules that associate data points to one another based on some measure between them [18, 19]. Increasingly, deep learning systems that make explicit use of pairwise similarities between neighboring samples within their training data are being developed. Systems such as SAINT update internal representations of tabular data via a row attention mechanism [20]. Other proposed methods employ similar strategies in domains such as image restoration [21], confidence estimation [22], and collaborative filtering [23]. In the domain of few-shot learning, matching networks use associations in data for prediction using pretrained models [24].

**Supervised Metric Learning** The primary aim of metric learning is to construct an embedding space where pairwise semantic relationships between input data are captured by a metric over the space [25]. In supervised metric learning, training examples are cast into pairwise constraints: the equivalence constraints where pairs of data points belong to the same classes, and inequivalence constraints where pairs of data points belong to different classes. Among the foundational algorithms in this field are Neighborhood Components Analysis (NCA) and Large Margin Nearest Neighbor

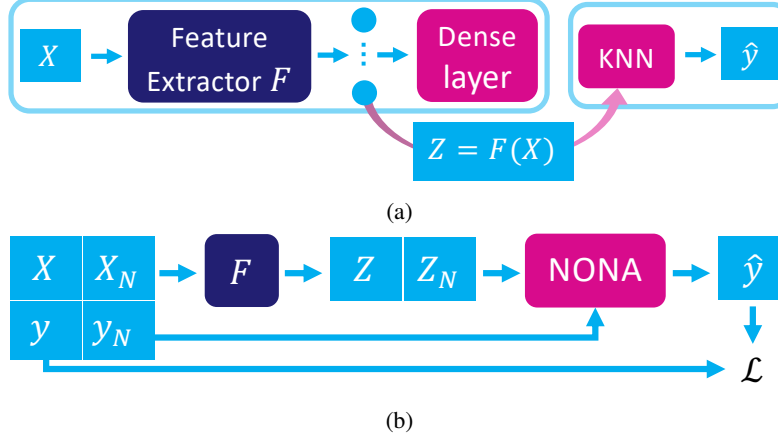


Figure 1: (a) depicts a typical two-stage supervised finetuning workflow and (b) the NONA regressor workflow. In two-stage supervised finetuning, the dense layer regressor used to finetune the upstream feature extractor is discarded, and a traditional regressor like k-NN is trained on the new embeddings. NONA finetunes the upstream feature extractor with a differentiable proxy of the k-NN algorithm and implicitly imposes metric learning constraints on the feature extractor’s output embeddings. See Figure 2 for a full description of the NONA block.

(LMNN) learning [26, 27], where the semantic similarity being pursued is class membership. NCA learns a linear transformation of data that minimizes the  $L_1$  distance between the true and predicted class distributions by maximizing a stochastic variant of leave-one-out k-NN. NCA has been adapted into neural networks by Qin et al. [28], where an NCA objective guides the construction of a neural network architecture. LMNN, on the other hand, makes no assumptions about the underlying distribution of data and instead learns a Mahalanobis distance metric that enforces nearest neighbors always belong to the same class while large margins separate data from different classes. The large margin principle has been adapted for deep neural networks by Elsayed et al. [29], where a novel loss function can enforce large margin metric learning in input, output, and hidden layers of neural networks. Strongly associated with these methods is the metric learning for kernel regression (MLKR) algorithm and its variants [30].

**Sparse Attention** Sparse attention is concerned with reducing the number of inputs attending to each other within a neural attention mechanism [31]. Besides reducing compute, the primary motivation behind these approaches is to develop attention mechanisms that are more selective. Traditional attention relies on the SoftMax function, which yields non-zero attention weights for all inputs [32]. A number of methods have been introduced to account for this, such as top-k attention [33], local windowing [34], Sparsek [35], and Reformer-based methods [36]. While these approaches limit the number of nonzero attention weights, many are non-differentiable. Consequently, they cannot be optimized effectively in the context of end-to-end deep learning. More sophisticated methods, such as Sparsemax [37], produce sparse outputs via a non-learned projection, but do not adapt to the semantic context of local densities of the embedding space.

### 3 Methods

Given a deep learning-based regression architecture, we refer to all components upstream from the regression head as the "feature extractor", denoted by  $F$ . For data and label pairings  $X \times y \subset \Omega \times \mathbb{R}$ , where  $\Omega$  is a sample space, the feature extractor embeds data via  $F(X) = Z \subset \mathbb{R}^d$  for an embedding dimension  $d$ .

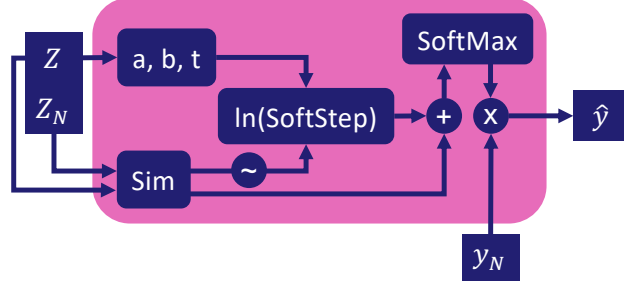


Figure 2: Block diagram of the NONA regression block with SoftStep learned attention-masking.  $Z$  and  $Z_N$  are the embeddings of prediction data,  $X$ , and neighbor data,  $X_N$ .  $Sim$  is the matrix of similarities between  $Z$  and  $Z_N$ . Learned SoftStep parameters are denoted  $a, b, t$ , and the  $\sim$  operation represents min-max normalization. SoftStep is applied to the normalized similarity matrix, and the un-normalized matrix is residually connected to the output before  $SoftMax$  is applied.  $y_N$  represents the true labels of  $X_N$  and  $\hat{y}$  is the vector of predicted labels for  $X$ .

### 3.1 Nearness of Neighbors Attention (NONA)

Let  $X \subset \Omega$  be a set of "prediction data" with  $|X| = b$  and let  $X_N \times y_N = \{(x_n, y_n)\}_{n=1}^N \subset \Omega \times \mathbb{R}$  be a labeled set of "neighbor" data. We define  $Z = F(X)$  and  $Z_N = F(X_N)$  respectively. Then,

$$\hat{y} = NONA(Z, Z_N, y_N) = SoftMax(Sim(Z, Z_N))y_N \quad (1)$$

where  $Sim(Z, Z_N) \in \mathbb{R}^{b \times N}$  with  $Sim(Z, Z_N)_{ij} = sim(z_i, z_{N_j})$  for some chosen similarity measure  $sim$ . On the sample level,  $\hat{y}_i = \sum_{j=1}^N p_{ij} y_j$  where  $p_{ij} = \frac{e^{sim(z_i, z_{N_j})}}{\sum_{k=1}^N e^{sim(z_i, z_{N_k})}}$  are attention weights. In traditional attention mechanisms,  $sim$  is often a scaled dot product similarity [32]. During training,  $X_n = X$  and self-similarities are masked by computing

$SoftMax(Sim(Z, Z_N) + M)y_N$  where  $M \in \mathbb{R}^{b \times b}$  with  $M_{ij} = \begin{cases} -\infty, & i = j \\ 0, & i \neq j \end{cases}$ . NONA is distinct

both as an attention mechanism and as an NCA prediction or k-NN variant, due to the novel learned similarity-masking scheme detailed in 3.2 as well as its natural compatibility with gradient descent-based optimization of the mean squared error (MSE) loss. As we show in section 4.1, the combination of NONA regression and MSE simultaneously drives regression performance and induces similarity structure in the embedding space without the need for explicit metric learning optimizations.

### 3.2 Learned attention masking with SoftStep

For bounded measures of similarity, such as negative  $L_p$  distance or dot product derived similarities, the above formulation of our differentiable neighbor-based regression layer, NONA, fails to exhibit a crucial aspect of the original k-NN regression algorithm. In k-NN, the labels of sufficiently dissimilar neighbors are rejected from the prediction entirely. In NONA, for bounded similarity measures and  $SoftMax$  based weighting, the label of every neighbor point to the embedding of a sample for prediction has some non-zero weight associated with it. Therefore, we desire similarity measures that achieve high dissimilarity, or even  $-\infty$  similarity, so that sufficiently dissimilar neighbors are masked out by the  $SoftMax$  operation.

While it is possible to introduce the traditional k as a "hard-mask" hyperparameter of NONA, the associated hyperparameter tuning would introduce high computational costs due to the non-differentiability of the k-neighbors selection algorithm. Specifically, for unweighted k-NN,

$$k\text{-NN}(x) = \frac{\sum_{i=1}^N mask(x_i) y_i}{\sum_{i=1}^N mask(x_i)} \text{ where } mask(x_i) = \begin{cases} 1, & rank(d(x, x_i)) \leq k \\ 0, & rank(d(x, x_i)) > k \end{cases}$$

As ranking is generally non-differentiable [38], and the outer step function has a zero derivative everywhere it is defined, this procedure is not generally incorporable into deep learning systems. Though differentiable ranking procedures do exist [39], they require solving complex optimization problems distinct from that of fitting a neural network for prediction.

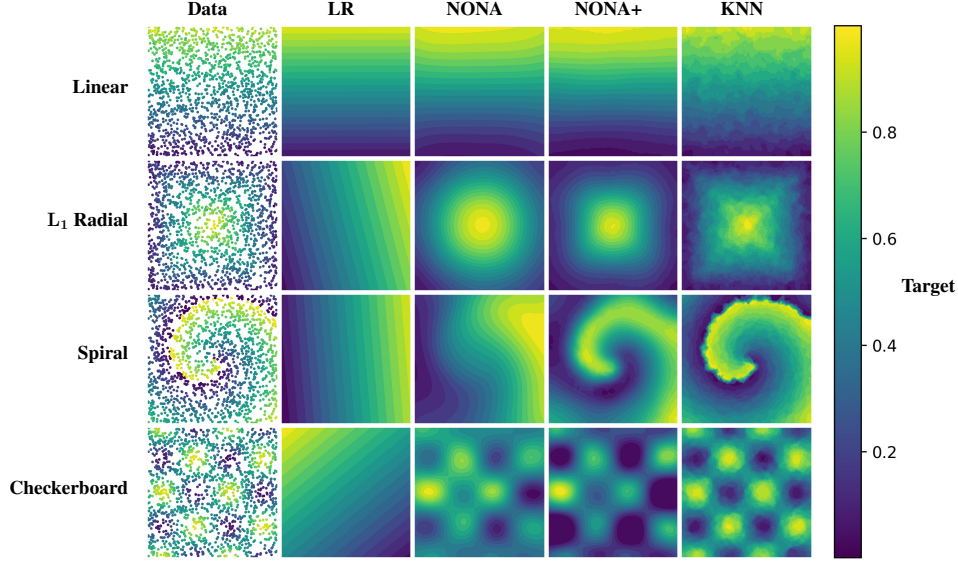


Figure 3: Synthetic datasets were generated by sampling points from the square domain  $[-1, 1]^2$  and assigning continuous labels using distinct target functions. The color gradients depict the target values and resulting regression surfaces learned by linear regression (LR), k-NN, NONA, and NONA with SoftStep (written as NONA+). LR cannot capture the nonlinear complexity of the radial, spiral, and checkerboard targets, whereas k-NN does not learn smooth regression surfaces. Conversely, NONA 3.1 and NONA with learned attention-masking 3.2 (NONA+) can learn smooth nonlinear regression surfaces that capture the underlying data structure. This capability relaxes the constraints on upstream neural network feature extractors during supervised finetuning.

While there are more sophisticated sparse-attention mechanisms than top-k selection in the literature, many are formulated in ways which make them less desirable for attention in the context of prediction. Sparsemax reflects local density by retaining more neighbors when similarity scores are uniform [37], but lacks awareness of how that density relates to predictive uncertainty or target variability. Prior work has shown that regions of equal density in feature space may warrant different neighbor selection strategies depending on local structure or semantic variation, underscoring the need for a context-sensitive masking approach [40, 41].

In order to achieve a sparse-attention mechanism that accounts for the full context of how data are distributed in the embedding space, we introduce a learned attention-masking scheme called SoftStep. SoftStep works by shifting all computed similarities to a given prediction point by a non-positive value via a learned function of said point prior to the application of the *SoftMax* function.

We augment NONA with SoftStep by applying it to the normalized similarity between a prediction point  $z^*$  and a neighbor point  $z$ , denoted as  $\text{Sim}(z^*, z)$ , via

$$\text{Sim}(z^*, z) \leftarrow \text{Sim}(z^*, z) + \ln(\text{SoftStep}(\overline{\text{Sim}(z^*, z)})) \quad (2)$$

prior to applying the *SoftMax* operation. We describe the full implementation of the SoftStep algorithm in Algorithm 1 and depict the NONA regression block with Softstep in Figure 2. Below we describe the specific functions used for shifting similarities in SoftStep.

### 3.2.1 SoftStep functions

Two formulations of the SoftStep function considered in this work are defined as follows:

$$S_1(x; a, b, t) = \begin{cases} 0, & 0 \leq x \leq a \\ \frac{(x-a)^{\frac{1}{t}}}{(x-a)^{\frac{1}{t}} + (b-x)^{\frac{1}{t}}}, & a < x < b \\ 1, & b \leq x \leq 1 \end{cases} \quad S_2(x; b, t) = \begin{cases} \frac{x}{b} \frac{(b-x)^{\frac{1}{t}}}{1-t}, & 0 \leq x < b \\ 1, & b \leq x \leq 1 \end{cases} \quad (3)$$

Here,  $a$  is a parameter that controls the threshold for rejecting neighbors based on their normalized similarities,  $b$  is a parameter that controls which neighbor similarities are completely preserved, and

$t$  is a parameter controlling the transition between these extreme regions.  $(a, b, t)$  may be realized as learned global parameters of the model or as point-dependent parameters of embeddings. In  $S_1$ , as the transition parameter  $t$  varies from 0 to 1, the mask varies between a step function at  $\frac{a+b}{2}$  and a double-clamped linear function joining the point  $(a, 0)$  to  $(b, 1)$ . In  $S_2$ , the mask varies between the constant 0 function and the constant 1 function on  $[0, b]$ .  $S_2$  cannot easily include a rejection parameter as  $\lim_{x \rightarrow 0} S_2'(x) = \infty$  for certain values of  $t$ . Appendix A shows the shape of  $S_1$  and  $S_2$  for various values of the transition parameter. We note that these families of functions are similar to *SmoothStep* functions which have been widely adopted in computer graphics [42].

The novelty of SoftStep comes from the real valued transition parameter  $t$  which allows tuning of the mask's shape during model training rather than making a hard-value selection in advance. To the best of our knowledge, functions of this form have not been used for attention-masking.

## 4 Theoretical Analysis

### 4.1 Embedding Structure Induced by NONA with MSE

We posit that a NONA model with MSE loss yields implicit optimization conditions for structuring pairs of points in the embedding space with respect to their labels, as well as conditions for structuring triplets of points. We observe that,

$$\begin{aligned}
\mathcal{L}(y, \hat{y}) &= \frac{1}{N} \sum_{i=1}^N (y_i - \text{NONA}(z_i, Z_N, y_N))^2 \\
&= \frac{1}{N} \sum_{i=1}^N (y_i - \sum_{j=1}^N p_{ij} y_j)^2 \\
&= \frac{1}{N} \sum_{i=1}^N (\sum_{j=1}^N (y_i - y_j) p_{ij})^2 && \text{since } \sum_{j=1}^N p_{ij} = 1 \\
&= \frac{1}{N} \sum_{i=1}^N (\sum_{j=1}^N \Delta_{ij}^2 p_{ij}^2 + 2 \sum_{j \neq k} \Delta_{ij} p_{ij} \Delta_{ik} p_{ik}) && \text{where } \Delta_{ij} := y_i - y_j
\end{aligned}$$

Terms of the form  $\Delta_{ij}^2 p_{ij}^2$  represent a pairwise similarity loss on the points indexed by  $(i, j)$ . Assigning  $j$  high proportional similarity to  $i$  accrues a penalty as an increasing function of the label distance.

Triplet terms  $\Delta_{ij} p_{ij} \Delta_{ik} p_{ik}$  also encode embedding conditions. However, a more illuminating description of the optimal triplet embedding geometry considers the partial optimization of terms of the form:

$$T_{ijk} = (\Delta_{ij} p_{ij} + \Delta_{ik} p_{ik})^2 \quad \text{subject to} \quad p_{ij} + p_{ik} = 1 - \sum_{l \neq j, k} p_{il} = R$$

This optimization analysis will yield different embedding conditions depending on the ordering of the labels  $j$  and  $k$  relative to the anchor point  $i$ . In the analysis of this local subproblem, we assume  $p_{il}$  is fixed for all  $l \neq j, k$  and that  $p_{ij}, p_{ik}$  are optimized independently. Additionally, our analysis only focuses on the case of NONA with SoftStep in which  $p_{ij}$  or  $p_{ik}$  may vanish. Analogous embedding conditions can be derived from a parallel analysis of NONA without SoftStep. We also limit our focus to the case where  $y_i \neq y_j \neq y_k$  as the triplet loss collapses into a simpler embedding condition if any of the labels are equal.

We proceed by minimizing  $T_{ijk}$  as a convex quadratic with respect to  $p_{ij}$  on the interval  $[0, R]$ .

$$T_{ijk}(p_{ij}) = (\Delta_{ij} p_{ij} + \Delta_{ik} (R - p_{ij}))^2 = ((\Delta_{ij} - \Delta_{ik}) p_{ij} + \Delta_{ik} R)^2$$

has the unconstrained minimizer  $p_{ij}^* = \frac{\Delta_{ik}}{\Delta_{ik} - \Delta_{ij}} R$ . From here we examine two cases based on the ordering of the three labels  $y_i, y_j, y_k$  that will yield two conditions depending on whether the anchor point label lies between the other two labels or is extreme itself.

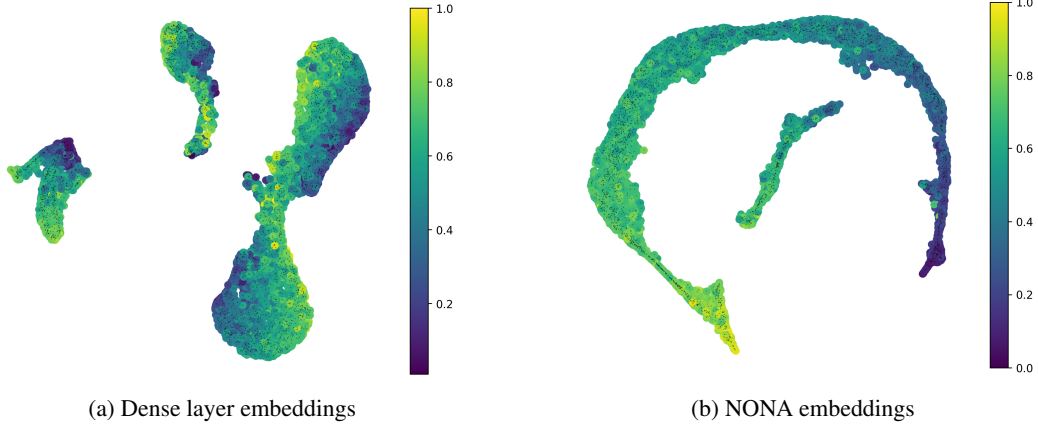


Figure 4: UMAP projections of RSNA training and test set embeddings colored by true label [43]. Black dots indicate a test point. (a) shows the embedding space yielded by dense layer regression; (b) shows the corresponding NONA model embeddings. NONA trained with MSE loss enforces local structure on embeddings that a dense layer does not. The fragmentation of the dense layer’s embeddings may explain why k-NN finetuned on dense embeddings significantly underperforms k-NN finetuned on NONA embeddings.

**Extreme anchor label:** If  $y_i < y_j < y_k$ , then  $p_{ij}^* > R$  and so  $T_{ijk}$  is minimized when  $p_{ij} = R$ , which implies  $p_{ik} = 0$ . That is, if the label of  $j$  is closer to that of  $i$  than the label of  $k$  is, then all the available proportional similarity between their embeddings is optimized to go to  $j$ . It can be seen that all arrangements of  $y_i, y_j, y_k$  in which  $y_i$  is extreme yield analogous conditions.

**Intermediate anchor label:** If  $y_j < y_i < y_k$  then  $0 < p_{ij}^* < R$  and thus is the true minimizer. The condition  $p_{ik} = R - p_{ij}$  yields that  $T_{ijk}$  is minimized when  $p_{ik} = \frac{\Delta_{ij}}{\Delta_{ij} + \Delta_{ik}} R$  and so optimality is achieved when

$$\frac{p_{ij}}{p_{ik}} = \frac{y_k - y_i}{y_i - y_j},$$

or when embedding similarity is distributed in *exact proportion* to label similarity. The same expression results from the case where  $y_k < y_i < y_j$ . Notice that the above analysis on triplets can be generalized to a quadratic program in as many as  $N$  dimensions, which suggests that higher order structures in the embedding space may be jointly optimized for as well. However, as we demonstrate in Appendix D, the solution to this more general optimization problem reduces to the triplet case: the available similarity is optimally allocated to the one or two neighbors whose labels are closest to the anchor’s, in proportion to their label differences.

#### 4.2 Embedding Space Constraints

Linear prediction assumes the existence of a data embedding in which representations are related to the target variable linearly with an error-minimizing constant variance [44]. This strong constraining assumption limits the expressiveness of the embedding space that the feature extractor can construct. As a result, rich structures such as multiplicative feature interactions [45], threshold effects [46], and curved manifolds like sinusoidal or spiral relationships cannot be captured by a simple affine map [47]. However, as a differentiable neighbor-based regression algorithm, NONA frees the upstream feature extractor to embed the data in more complex arrangements that may better preserve the predictive signal within the data. In Figure 3 we demonstrate empirically that the NONA is capable of capturing nonlinear relationships between data and a target variable.

### 5 Experiments

We measure the regression performance of several configurations of the NONA algorithm, as well as its formulations with the learned masking scheme SoftStep, using several unstructured datasets for

| Dataset             | Dense Layer       | Dense + k-NN      | NONA                               | NONA + k-NN                         |
|---------------------|-------------------|-------------------|------------------------------------|-------------------------------------|
| RSNA [51]           | $5.12 \pm 0.608$  | $5.56 \pm 0.458$  | $4.13 \pm 0.235$                   | <b><math>4.03 \pm 0.183</math></b>  |
| MedSegBench [52]    | $6.69 \pm 1.29$   | $7.37 \pm 1.15$   | $4.02 \pm 0.608$                   | <b><math>2.38 \pm 0.356</math></b>  |
| ADReSSo [53]        | $96.2 \pm 33.3$   | $41.3 \pm 7.36$   | $28.0 \pm 4.13$                    | <b><math>24.8 \pm 2.17</math></b>   |
| CoughVid [54]       | $39.7 \pm 27.0$   | $23.2 \pm 0.370$  | <b><math>21.2 \pm 0.195</math></b> | $23.2 \pm 0.551$                    |
| NoseMic [55]        | $7.96 \pm 0.947$  | $7.23 \pm 0.607$  | $6.01 \pm 0.472$                   | <b><math>5.89 \pm 0.672</math></b>  |
| Udacity [56]        | $0.435 \pm 0.170$ | $0.732 \pm 0.250$ | $0.358 \pm 0.104$                  | <b><math>0.239 \pm 0.060</math></b> |
| Pitchfork [57]      | $69.6 \pm 167.0$  | $14.8 \pm 2.20$   | <b><math>10.2 \pm 1.01</math></b>  | $10.5 \pm 1.65$                     |
| Houses [58]         | $303 \pm 81.3$    | $20.0 \pm 1.90$   | <b><math>13.2 \pm 1.77</math></b>  | $14.7 \pm 1.38$                     |
| Books [Appendix C]  | $8.33 \pm 0.680$  | $7.96 \pm 0.58$   | $7.48 \pm 0.588$                   | <b><math>7.48 \pm 0.55</math></b>   |
| Austin [Appendix C] | $2.29 \pm 0.216$  | $2.26 \pm 0.177$  | <b><math>2.05 \pm 0.231</math></b> | $2.06 \pm 0.217$                    |

Table 1: Average mean squared error (MSE)  $\pm$  standard deviation across methods over ten random splits of each dataset. The best mean results for each dataset are in bold. We use "+ k-NN" to indicate the performance of a tuned k-NN regressor on the final SFT embeddings of the corresponding model. All measurements have been scaled by  $10^3$  for readability. A complete description of each dataset, along with all preprocessing pipelines and feature extractors can be found in Appendix C. The median MSE reduction from dense layer prediction to NONA is 32.2%. NONA yielded the best performance on 4 of 10 datasets and NONA + k-NN did so on the remaining 6 of 10.

regression. Each unstructured dataset is paired with a pretrained neural network feature extractor and finetuned in a supervised manner. All datasets are split 80/20 into development and testing, with the development set further split 85/15 into training and validation. Early stopping is performed when MSE performance does not improve on the validation set for 10 epochs. This procedure is repeated 10 times to get an average performance of each model. All training was conducted on a high performance compute cluster equipped with NVIDIA H100 Tensor Core GPUs, with each model trained individually on each fold of data using a single NVIDIA H100 SXM5 80GB GPU for a maximum of 48 hours [48].

Downstream of each feature extractor, a multilayer perceptron with hidden dimension 200 projects samples to a 25 dimensional embedding space, followed by one of the following regression heads: a dense layer; k-NN trained on the embeddings upstream of the dense layer; NONA; k-NN trained on the embeddings upstream of NONA. For all experiments, k-NN was fit using grid parameters  $k \in \{3, 5, 7\}$ ,  $p \in \{1, 2\}$ , and weights  $\in \{\text{uniform, distance}\}$  using scikit-learn 1.6.1 [49].

## 6 Results

Across the evaluation, either NONA or its two-stage SFT with k-NN counterpart performs best in terms of average MSE. The results of our experiments can be found in Table 1. Friedman testing with posthoc Nemenyi correction, based on mean performance across datasets, reveals statistically significant performance differences ( $p < 0.05$ ) between NONA-based approaches and dense-based approaches (Figure 5) [50]. No statistically significant difference was found between NONA and NONA+k-NN nor between dense and dense+k-NN.

### 6.1 Ablation Study

We perform a serialized ablation on key aspects of our algorithm to determine the proper configuration for testing. The ablation is performed with respect to the RSNA dataset. Full results of our ablation study can be found in Appendix B. First, we ablate the similarity measure used within NONA. We study  $-L_2$  and  $-L_1$  distance as well as cosine and dot product similarity. Next, we ablate the SoftStep configuration. We study the  $S_1$  and  $S_2$  soft step function families in combination with point-wise learned masking parameters and global parameters, as well as NONA without SoftStep. We identify batch size as a potentially important parameter due to NONA’s reliance on the entire batch for prediction during training. As the third step in our ablation, we study the effect of the batch sizes (32, 64, 128, 256). Finally, we study how performance varies as a function of embedding dimensions 25, 50, and 100. This exploration yields the parameter combination:  $-L_2$  similarity,  $S_2$  SoftStep with point-wise parameters, a batch size of 32, and embedding dimension of 25. We use these parameters in all experiments comparing NONA to the dense layer benchmark.



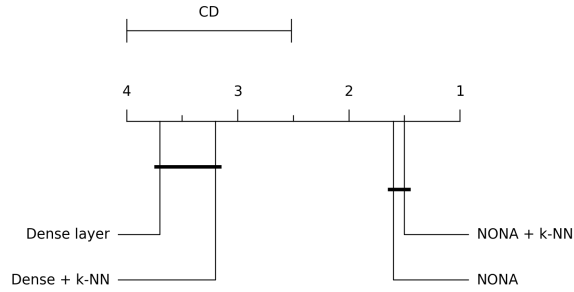


Figure 5: Critical distance (CD) plot from Friedman testing, based on mean performance across datasets, reveals significant differences between regressors. NONA significantly outperforms both the dense regressor ( $p = 0.0016$ ) and its corresponding k-NN variant ( $p = 0.0286$ ). Similarly, k-NN finetuned on embeddings produced by NONA significantly outperforms the dense regressor ( $p = 0.0008$ ) and the k-NN variant trained on dense embeddings ( $p = 0.0171$ ). No significant difference is observed between NONA and its associated k-NN variant ( $p = 0.9982$ ), nor between the dense regressor and its k-NN variant ( $p = 0.8224$ ).

## 7 Discussion

Our results demonstrate that NONA is a viable and expressive alternative to conventional regression with dense layers in deep learning systems. By removing the constraint that learned representations relate to the target through a global linear function, NONA enables feature extractors to explore a broader class of embedding geometries that are only locally constrained to embed similarly labeled points similarly. This flexibility allows the model to potentially capture more predictive signals in the data and better align embeddings with semantics that are relevant to the task. This distinction is illustrated in Figure 4, which demonstrates that NONA is able to achieve improved performance specifically by learning a nonlinear regression surface.

A central contribution of this work is the characterization of the precise geometric conditions being optimized for by NONA with MSE loss. This model and loss pairing encourages embeddings in which similarly labeled points are attracted, and dissimilarly labels are repelled, in proportion to their label differences, thereby realizing MSE as a metric learning objective in this context. The visually apparent structuring of data relative to labels shown in Figure 4 demonstrates the effectiveness of our formulation. Notably, NONA with MSE is distinct from commonly-used triplet and contrastive loss formulations where separate optimization problems need to be explicitly solved with respect to all viable pairs and triplets of points. It is more similar to MLKR ([30]) incorporated into the end-to-end optimization context of an arbitrary deep learning system. The formulation of SoftStep also distinguishes NONA from similar kernel regression methods. Despite the promise of NONA with MSE, further research is warranted. As we demonstrated in our analysis, the optimization conditions yielded by the MSE loss are only pairwise and triplet in nature. Further mathematical insight is needed to uncover possible higher order conditions, if any are present. If the current optimization is limited to co-structuring pairs and triplets, investigations into augmenting MSE may yield conditions for higher order embedding structure.

Our ablation study shows that SoftStep is a useful addition to our algorithm (see Appendix B for a more detailed description). However, it is notable that tuning a traditional k-NN algorithm to the final NONA embeddings tends to improve performance, albeit insignificantly (Table 1, Figure 5). This may be due to the lack of a k-NN-like rejection parameter in  $S_2$ , the function family yielded by the ablation. Alternatively, the choice to mask normalized similarities rather than similarity rankings, as in k-NN, may hinder performance. Future work may include exploring these augmentations and comparing to pre-existing sparse attention approaches.

Other potential avenues for future research include integrating NONA with upstream self-similarity blocks such as [20, 21], interpretation via attention maps, multi-head approaches and  $Q, K, V$  transformations, similar to [24], and regression head ensembling.

## 8 Conclusion

In this work we propose Nearness of Neighbors Attention (NONA), a novel differentiable proxy of k-NN well-suited for supervised finetuning on regression tasks using unstructured data. We also propose SoftStep, a novel family of differentiable, parameterized attention-masking functions. Theoretical analysis demonstrates that NONA paired with MSE loss imposes pairwise and triplet loss constraints on neural network embeddings in proportion to the label difference between data. Regression experiments on several unstructured datasets show that NONA paired with SoftStep significantly outperforms dense layer regressors as well as two-stage finetuning with a k-nearest neighbors regression head.

## References

- [1] Ting Chen, Simon Kornblith, Kevin Swersky, Mohammad Norouzi, and Geoffrey E Hinton. Big self-supervised models are strong semi-supervised learners. *Advances in neural information processing systems*, 33:22243–22255, 2020.
- [2] Alireza Maleki, Mohammad Raahemi, and Hamid Nasiri. Breast cancer diagnosis from histopathology images using deep neural network and xgboost. *Biomedical Signal Processing and Control*, 86:105152, 2023.
- [3] Anurag Tiwari and Amrita Chaturvedi. A multiclass eeg signal classification model using spatial feature extraction and xgboost algorithm. In *2019 IEEE/RSJ International Conference on Intelligent Robots and Systems (IROS)*, pages 4169–4175. IEEE, 2019.
- [4] Anonymous. Anonymized for peer review, Anonymous.
- [5] Ravid Shwartz-Ziv and Amitai Armon. Tabular data: Deep learning is not all you need. *Information Fusion*, 81:84–90, 2022.
- [6] Kiran Adnan and Rehan Akbar. An analytical study of information extraction from unstructured and multidimensional big data. *Journal of Big Data*, 6(1):1–38, 2019.
- [7] Ehsan Amid, Rohan Anil, Wojciech Kotłowski, and Manfred K Warmuth. Learning from randomly initialized neural network features. *arXiv preprint arXiv:2202.06438*, 2022.
- [8] Jordi Pons and Xavier Serra. Randomly weighted cnns for (music) audio classification. In *ICASSP 2019-2019 IEEE international conference on acoustics, speech and signal processing (ICASSP)*, pages 336–340. IEEE, 2019.
- [9] Stephen Notley and Malik Magdon-Ismail. Examining the use of neural networks for feature extraction: A comparative analysis using deep learning, support vector machines, and k-nearest neighbor classifiers. *arXiv preprint arXiv:1805.02294*, 2018.
- [10] Nima Tajbakhsh, Jae Y Shin, Suryakanth R Gurudu, R Todd Hurst, Christopher B Kendall, Michael B Gotway, and Jianming Liang. Convolutional neural networks for medical image analysis: Full training or fine tuning? *IEEE transactions on medical imaging*, 35(5):1299–1312, 2016.
- [11] Newton Spolaôr, Huei Diana Lee, Ana Isabel Mendes, Conceição Veloso Nogueira, Antonio Rafael Sabino Parmezan, Weber Shoitzy Resende Takaki, Claudio Saddy Rodrigues Coy, Feng Chung Wu, and Rui Fonseca-Pinto. Fine-tuning pre-trained neural networks for medical image classification in small clinical datasets. *Multimedia Tools and Applications*, 83(9): 27305–27329, 2024.
- [12] Ian Pan, Hans Henrik Thodberg, Safwan S Halabi, Jayashree Kalpathy-Cramer, and David B Larson. Improving automated pediatric bone age estimation using ensembles of models from the 2017 rsna machine learning challenge. *Radiology: Artificial Intelligence*, 1(6):e190053, 2019.
- [13] Saturnino Luz, Fasih Haider, Sofia de la Fuente Garcia, Davida Fromm, and Brian MacWhinney. Alzheimer’s dementia recognition through spontaneous speech, 2021.

- [14] Aparna Balagopalan and Jekaterina Novikova. Comparing acoustic-based approaches for alzheimer’s disease detection. In *Proc. Interspeech 2021*, pages 3800–3804, 2021.
- [15] Brady Laska, Pengcheng Xi, Julio J. Valdés, Bruce Wallace, and Rafik Goubran. Zero-shot multi-task cough sound analysis with speech foundation model embeddings. In *2024 IEEE International Symposium on Medical Measurements and Applications (MeMeA)*, pages 1–6, 2024. doi: 10.1109/MeMeA60663.2024.10596816.
- [16] Maryam Zolnoori, Ali Zolnour, and Maxim Topaz. Adscreen: A speech processing-based screening system for automatic identification of patients with alzheimer’s disease and related dementia. *Artificial intelligence in medicine*, 143:102624, 2023.
- [17] Maya K Nachesa and Vlad Niculae. knn for whisper and its effect on bias and speaker adaptation. In *Findings of the Association for Computational Linguistics: NAACL 2025*, pages 6621–6627, 2025.
- [18] Evelyn Fix. *Discriminatory analysis: nonparametric discrimination, consistency properties*, volume 1. USAF school of Aviation Medicine, 1985.
- [19] Thomas Cover and Peter Hart. Nearest neighbor pattern classification. *IEEE transactions on information theory*, 13(1):21–27, 1967.
- [20] Gowthami Somepalli, Micah Goldblum, Avi Schwarzschild, C Bayan Bruss, and Tom Goldstein. Saint: Improved neural networks for tabular data via row attention and contrastive pre-training. *arXiv preprint arXiv:2106.01342*, 2021.
- [21] Tobias Plötz and Stefan Roth. Neural nearest neighbors networks. *Advances in Neural information processing systems*, 31, 2018.
- [22] Nicolas Papernot and Patrick McDaniel. Deep k-nearest neighbors: Towards confident, interpretable and robust deep learning. *arXiv preprint arXiv:1803.04765*, 2018.
- [23] Xiangnan He, Lizi Liao, Hanwang Zhang, Liqiang Nie, Xia Hu, and Tat-Seng Chua. Neural collaborative filtering. In *Proceedings of the 26th international conference on world wide web*, pages 173–182, 2017.
- [24] Oriol Vinyals, Charles Blundell, Timothy Lillicrap, Daan Wierstra, et al. Matching networks for one shot learning. *Advances in neural information processing systems*, 29, 2016.
- [25] Liu Yang and Rong Jin. Distance metric learning: A comprehensive survey. *Michigan state universiy*, 2(2):4, 2006.
- [26] Jacob Goldberger, Geoffrey E Hinton, Sam Roweis, and Russ R Salakhutdinov. Neighbourhood components analysis. *Advances in neural information processing systems*, 17, 2004.
- [27] Kilian Q Weinberger, John Blitzer, and Lawrence Saul. Distance metric learning for large margin nearest neighbor classification. *Advances in neural information processing systems*, 18, 2005.
- [28] Chen Qin, Shiji Song, and Gao Huang. Non-linear neighborhood component analysis based on constructive neural networks. In *2014 IEEE International Conference on Systems, Man, and Cybernetics (SMC)*, pages 1997–2002. IEEE, 2014.
- [29] Gamaleldin Elsayed, Dilip Krishnan, Hossein Mobahi, Kevin Regan, and Samy Bengio. Large margin deep networks for classification. *Advances in neural information processing systems*, 31, 2018.
- [30] Kilian Q Weinberger and Gerald Tesauro. Metric learning for kernel regression. In *Artificial intelligence and statistics*, pages 612–619. PMLR, 2007.
- [31] Yi Tay, Dara Bahri, Liu Yang, Donald Metzler, and Da-Cheng Juan. Sparse sinkhorn attention. In *International conference on machine learning*, pages 9438–9447. PMLR, 2020.

- [32] Ashish Vaswani, Noam Shazeer, Niki Parmar, Jakob Uszkoreit, Llion Jones, Aidan N Gomez, Łukasz Kaiser, and Illia Polosukhin. Attention is all you need. *Advances in neural information processing systems*, 30, 2017.
- [33] Ankit Gupta, Guy Dar, Shaya Goodman, David Ciprut, and Jonathan Berant. Memory-efficient transformers via top- $k$  attention. *arXiv preprint arXiv:2106.06899*, 2021.
- [34] Thanh-Tung Nguyen, Xuan-Phi Nguyen, Shafiq Joty, and Xiaoli Li. Differentiable window for dynamic local attention. *arXiv preprint arXiv:2006.13561*, 2020.
- [35] Chao Lou, Zixia Jia, Zilong Zheng, and Kewei Tu. Sparser is faster and less is more: Efficient sparse attention for long-range transformers. *arXiv preprint arXiv:2406.16747*, 2024.
- [36] Nikita Kitaev, Łukasz Kaiser, and Anselm Levskaya. Reformer: The efficient transformer. *arXiv preprint arXiv:2001.04451*, 2020.
- [37] Andre Martins and Ramon Astudillo. From softmax to sparsemax: A sparse model of attention and multi-label classification. In *International conference on machine learning*, pages 1614–1623. PMLR, 2016.
- [38] Mathieu Blondel, Olivier Teboul, Quentin Berthet, and Josip Djolonga. Fast differentiable sorting and ranking. In *International Conference on Machine Learning*, pages 950–959. PMLR, 2020.
- [39] Felix Petersen, Hilde Kuehne, Christian Borgelt, and Oliver Deussen. Differentiable top- $k$  classification learning. In *International Conference on Machine Learning*, pages 17656–17668. PMLR, 2022.
- [40] Mohammad Chehreghani and Mohammad Reza Chehreghani. Context-sensitive knn search for high-dimensional data. In *Proceedings of the 27th ACM International Conference on Information and Knowledge Management (CIKM)*, pages 1505–1514, 2018.
- [41] Jian Wang, Hua Li, and Lin Zhang. Learning feature space density for improved neighbor selection in regression tasks. In *Proceedings of the IEEE/CVF Conference on Computer Vision and Pattern Recognition (CVPR)*, pages 1234–1243, 2023.
- [42] Hussein Hazimeh and Rahul Mazumder. Fast and accurate sparse regression via oracle. *Proceedings of the 37th International Conference on Machine Learning*, 119:4207–4216, 2020.
- [43] Leland McInnes, John Healy, and James Melville. Umap: Uniform manifold approximation and projection for dimension reduction. *arXiv preprint arXiv:1802.03426*, 2018.
- [44] Douglas C Montgomery, Elizabeth A Peck, and G Geoffrey Vining. *Introduction to linear regression analysis*. John Wiley & Sons, 2021.
- [45] R. J. Batista, C. A. Silva, and I. G. Costa. Efficient epistasis detection via cartesian interaction modelling. *Bioinformatics*, 40(5):831–838, 2024.
- [46] Zhiyi Su, Yulia R. Gel, and Joseph L. Gastwirth. The chngpt r package for threshold regression modelling. *Journal of Statistical Software*, 76(1):1–32, 2017.
- [47] Zhicheng Liang, Ming Li, He Fan, and Xiaoqian Zhang. Cyclum: inference of periodic pseudotime from single-cell rna-seq data via circular latent embedding. *Bioinformatics*, 36(11): 3320–3327, 2020.
- [48] Patricia Kovatch, Lili Gai, Hyung Min Cho, Eugene Fluder, and Dansha Jiang. Optimizing high-performance computing systems for biomedical workloads. In *2020 IEEE International Parallel and Distributed Processing Symposium Workshops (IPDPSW)*, pages 183–192. IEEE, 2020.
- [49] F. Pedregosa, G. Varoquaux, A. Gramfort, V. Michel, B. Thirion, O. Grisel, M. Blondel, P. Prettenhofer, R. Weiss, V. Dubourg, J. Vanderplas, A. Passos, D. Cournapeau, M. Brucher, M. Perrot, and E. Duchesnay. Scikit-learn: Machine learning in Python. *Journal of Machine Learning Research*, 12:2825–2830, 2011.

- [50] Janez Demšar. Statistical comparisons of classifiers over multiple data sets. *Journal of Machine learning research*, 7(Jan):1–30, 2006.
- [51] Safwan S Halabi, Luciano M Prevedello, Jayashree Kalpathy-Cramer, Artem B Mamonov, Alexander Bilbily, Mark Cicero, Ian Pan, Lucas Araújo Pereira, Rafael Teixeira Sousa, Nitamar Abdala, et al. The rsna pediatric bone age machine learning challenge. *Radiology*, 290(2): 498–503, 2019.
- [52] Zeki Kuş and Musa Aydin. Medsegbench: A comprehensive benchmark for medical image segmentation in diverse data modalities. *Scientific Data*, 11(1):1283, 2024. doi: 10.1038/s41597-024-04159-2. URL <https://doi.org/10.1038/s41597-024-04159-2>.
- [53] Saturnino Luz, Fasih Haider, Sofia de la Fuente, Davida Fromm, and Brian MacWhinney. Detecting cognitive decline using speech only: The addresso challenge. In *INTERSPEECH 2021*. ISCA, 2021.
- [54] Lara Orlandic, Tomas Teijeiro, and David Atienza. The coughvid crowdsourcing dataset, a corpus for the study of large-scale cough analysis algorithms. *Scientific Data*, 8(1):156, 2021.
- [55] Kayla-Jade Butkow, Ting Dang, Andrea Ferlini, Dong Ma, Yang Liu, and Cecilia Mascolo. An evaluation of heart rate monitoring with in-ear microphones under motion. *Pervasive and Mobile Computing*, 100:101913, 2024.
- [56] Shuyang Du, Haoli Guo, and Andrew Simpson. Self-driving car steering angle prediction based on image recognition. *arXiv preprint arXiv:1912.05440*, 2019.
- [57] Anthony T Pinter, Jacob M Paul, Jessie Smith, and Jed R Brubaker. P4kxspotify: A dataset of pitchfork music reviews and spotify musical features. In *Proceedings of the International AAAI Conference on Web and Social Media*, volume 14, pages 895–902, 2020.
- [58] Eman Ahmed and Mohamed Moustafa. House price estimation from visual and textual features. *arXiv preprint arXiv:1609.08399*, 2016.
- [59] Kaiming He, Xiangyu Zhang, Shaoqing Ren, and Jian Sun. Deep residual learning for image recognition. In *Proceedings of the IEEE conference on computer vision and pattern recognition*, pages 770–778, 2016.
- [60] Jin He and Dan Jiang. Fully automatic model based on se-resnet for bone age assessment. *IEEE access*, 9:62460–62466, 2021.
- [61] V Sanh. Distilbert, a distilled version of bert: smaller, faster, cheaper and lighter. In *Proceedings of Thirty-third Conference on Neural Information Processing Systems (NIPS2019)*, 2019.
- [62] Ahmed Rizk, Gwenaél Paul, Sylvain Incardona, Jean-Christophe Bugnard, Jean-Baptiste Besse, Jean-Christophe Salamero, and Jean-Christophe Olivo-Marin. Segmentation and quantification of subcellular structures in fluorescence microscopy images using squassh. *Nature Protocols*, 9(3):586–596, 2014. doi: 10.1038/nprot.2014.037. URL <https://www.nature.com/articles/nprot.2014.037>.
- [63] Mingxing Tan and Quoc Le. Efficientnet: Rethinking model scaling for convolutional neural networks. In *International conference on machine learning*, pages 6105–6114. PMLR, 2019.
- [64] Wei-Ning Hsu, Benjamin Bolte, Yao-Hung Hubert Tsai, Kushal Lakhotia, Ruslan Salakhutdinov, and Abdelrahman Mohamed. Hubert: Self-supervised speech representation learning by masked prediction of hidden units. *IEEE/ACM transactions on audio, speech, and language processing*, 29:3451–3460, 2021.
- [65] Zongyao Feng, Konstantin Markov, Junpei Saito, and Tomoko Matsui. Neural cough counter: A novel deep learning approach for cough detection and monitoring. *IEEE Access*, 2024.
- [66] Alec Radford, Jong Wook Kim, Tao Xu, Greg Brockman, Christine McLeavey, and Ilya Sutskever. Robust speech recognition via large-scale weak supervision. In *International conference on machine learning*, pages 28492–28518. PMLR, 2023.

- [67] Benjamin Warner, Antoine Chaffin, Benjamin Clavié, Orion Weller, Oskar Hallström, Said Taghadouini, Alexis Gallagher, Raja Biswas, Faisal Ladhak, Tom Aarsen, et al. Smarter, better, faster, longer: A modern bidirectional encoder for fast, memory efficient, and long context finetuning and inference. *arXiv preprint arXiv:2412.13663*, 2024.

## A Appendix: SoftStep Details

Here we provide the SoftStep algorithm. Additionally, the figure below shows the  $S_1$  and  $S_2$  families of SoftStep functions for various values of the  $t$  transition parameter.

---

### Algorithm 1 SoftStep Module

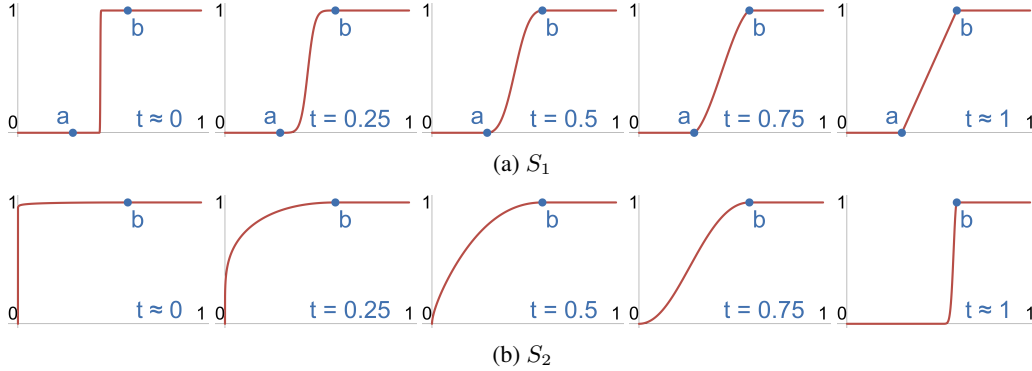
---

```

1: procedure SOFTSTEP( $Z, Z_N$ , SoftStep_fn, param_mode)
  Initialization (run once at module construction):
2:   if param_mode == "pointwise" then
3:     params  $\leftarrow$  Linear layer with sigmoid activation
4:   else if param_mode == "global" then
5:     params  $\leftarrow$  Learnable model-level parameters
6:   end if
7:   Store SoftStep_fn
  Forward Pass:
8:   if param_mode == "pointwise" then
9:      $(a_0, b_0, t) \leftarrow$  params( $Z$ )
10:  else if param_mode == "global" then
11:     $(a_0, b_0, t) \leftarrow \sigma(\text{params})$ 
12:  end if
13:   $\text{sim} \leftarrow \text{SIM}(Z, Z_N)$   $\triangleright$  Matrix of similarities
14:   $\text{sim\_norm} \leftarrow \text{NORM}(\text{sim})$   $\triangleright$  Normalize to  $[0, 1]$ 
15:  if SoftStep_fn requires  $a$  then
16:    if  $Z_N == Z$  (training) then
17:       $\text{top\_sim} \leftarrow$  row-wise max of  $\text{sim\_norm}$  excluding diagonal
18:    else
19:       $\text{top\_sim} \leftarrow$  row-wise max of  $\text{sim\_norm}$ 
20:    end if
21:     $a \leftarrow \min(a_0, \text{top\_sim}) - \epsilon$   $\triangleright \epsilon > 0$  small
22:     $b \leftarrow a + b_0 \cdot (1 - a)$ 
23:  else
24:     $a \leftarrow a_0$ 
25:     $b \leftarrow b_0$ 
26:  end if
27:   $\text{mask} \leftarrow \text{SoftStep\_fn}(\text{sim\_norm}, a, b, t)$ 
28:  return  $\text{sim} + \log(\text{mask})$ 
29: end procedure

```

---



Supplementary Figure A: Shape of the  $S_1$  and  $S_2$  SoftStep functions as the transition parameter  $t$  varies from 0 to 1. Both  $S_1$  and  $S_2$  are families of increasing surjective functions mapping the unit interval to itself.

## B Appendix: Ablation Study Results

We conduct ablation studies on both the NONA and dense layer prediction-based models used in our evaluation. We use the RSNA [51] dataset for our ablation and then apply the resulting configurations for experiments on all other datasets. In our ablation we evaluate on 3 random splits of the data for every configuration, whereas in the full experimentation we evaluate on 10. All MSE scores below are scaled by  $10^3$  for readability.

### B.1 NONA ablation

We conduct a serialized ablation on similarity measures, SoftStep functions, batch sizes, and embedding dimensions. Until ablated, Softstep is excluded, batch size is fixed at 128, and embedding dimension is fixed at 50.

| $-L_1$           | $-L_2$                             | dot              | cos              |
|------------------|------------------------------------|------------------|------------------|
| $6.11 \pm 0.382$ | <b><math>5.80 \pm 0.444</math></b> | $12.1 \pm 0.337$ | $12.5 \pm 0.240$ |

(a) Similarity measures

↓

| $S_1$ Global     | $S_1$ Pointwise  | $S_2$ Global     | $S_2$ Pointwise                    |
|------------------|------------------|------------------|------------------------------------|
| $5.94 \pm 0.333$ | $6.27 \pm 0.377$ | $5.51 \pm 0.935$ | <b><math>4.94 \pm 0.252</math></b> |

(b) SoftStep functions

↓

| 32                                 | 64               | 128              | 256              |
|------------------------------------|------------------|------------------|------------------|
| <b><math>4.45 \pm 0.105</math></b> | $4.83 \pm 0.212$ | $4.94 \pm 0.252$ | $5.17 \pm 0.210$ |

(c) Batch sizes

↓

| 25                                 | 50               | 100              |
|------------------------------------|------------------|------------------|
| <b><math>4.14 \pm 0.235</math></b> | $4.45 \pm 0.105$ | $4.23 \pm 0.244$ |

(d) Embedding dimensions

### B.2 Dense layer ablation

Among the ablated parameters given above, only batch size and embedding dimension apply to the dense layer benchmark. We conduct a full ablation, comparing all combinations of these parameters. The results of that ablation are given here.

| Embed\Batch | 32                                 | 64               | 128              | 256               |
|-------------|------------------------------------|------------------|------------------|-------------------|
| 25          | <b><math>5.08 \pm 0.322</math></b> | $6.46 \pm 0.716$ | $5.50 \pm 0.414$ | $10.1 \pm 0.568$  |
| 50          | $5.35 \pm 0.466$                   | $5.61 \pm 0.596$ | $7.90 \pm 0.821$ | $9.42 \pm 0.0690$ |
| 100         | $5.95 \pm 0.498$                   | $7.55 \pm 0.196$ | $6.80 \pm 1.15$  | $9.07 \pm 0.664$  |

Table 2: MSE across embedding dimensions (rows) and batch sizes (columns).



## C Appendix: Datasets and Feature Extractors

Exact model versions and pretrained weights are specified in the included GitHub repository. We ensured that at least two distinct feature extractors were chosen per unstructured modality (text, audio, and image) to demonstrate the generalizability of our proposed algorithm.

**RSNA Bone Age Prediction** The Radiological Society of North America (RSNA) Pediatric Bone Age Machine Learning Challenge collected pediatric hand radiographs labeled with the age of the subject in months [51]. We collected 14,036 images from this dataset. Images were resized to 224x224 pixels, normalized with mean and standard deviation of 0.5 across the single gray-scale channel and input to ResNet-18 pretrained on ImageNet [59, 60].<sup>1</sup>

**ADReSSo** The Alzheimer’s Dementia Recognition through Spontaneous Speech only (ADReSSo) diagnosis dataset has 237 audio recordings of participants undergoing the Cookie Thief cognitive assessment labeled with their score on the Mini Mental State Exam [53]. Transcripts of these recordings were tokenized and input to DistilBERT-base-uncased [61, 16].<sup>2</sup>

**MedSegBench** The MedSegBench BriFiSegMSBench dataset is comprised of single-channel microscopy images and corresponding segmentation masks [52]. We estimated the size of segmentation mask areas using EfficientNet trained on ImageNet. [62, 63].<sup>3</sup>

**CoughVid** The CoughVid dataset provides over 25,000 crowdsourced cough recordings, with 6,250 recordings labeled with participant age in years [54]. One second of cough audio was input to HuBERT pretrained on LibriSpeech and mean-pooled across time [64, 65].<sup>4</sup>

**NoseMic** The NoseMic dataset collected 1,297 30-second audio recordings of heart rate-induced sounds in the ear canal using an in-ear microphone under several activities [55]. Audio clips were denoised,<sup>5</sup> encoded with the Whisper tiny audio encoder [66], and mean-pooled across time.<sup>6</sup>

**Udacity** The Udacity self-driving car dataset is comprised of dashcam videos labeled with the angle of the car’s steering wheel [56]. Videos were downsampled to 4 frames per second for a total of 6,762 images and individual frames were input to EfficientNet trained on ImageNet [63].<sup>3</sup>

**Pitchfork** 24,649 reviews from the website Pitchfork were collected [57], where albums are scored from 0 to 10 in 0.1 increments. 1,500 randomly selected reviews were tokenized and input to BERT base [67].<sup>7</sup>

**Houses** The Houses dataset collects 535 curbside images of houses as well as their log-scaled list price [58]. Images were resized to 256x256 pixels, center cropped to 224x224, ImageNet normalized, and input to ResNet-34 [59].<sup>1</sup>

**Books** The MachineHack Book Price Prediction dataset collated 6237 synopses of books labeled with their log-normalized price.<sup>8</sup> Synopses were tokenized and input to DistilBERT-base-uncased.<sup>2</sup>

**Austin** The Kaggle Austin Housing Prices dataset collects over 15000 descriptions of homes labeled with their log-scaled list price.<sup>9</sup> Descriptions were tokenized and input to DistilBERT-base-uncased.<sup>2</sup>

## D Appendix: Higher Order Embedding Structure with NONA + MSE

We showed through an argument in Section 4.1 that the combination of NONA and MSE loss implicitly imposes optimization conditions on all pairs and triplets of embeddings. However, the setup of our argument is general for substructures of all orders within the embedding space. It is natural then to explore whether our argument yields embedding conditions on such higher order structures. We briefly show here that the analogous argument does not yield a unique embedding condition for structures beyond triplets regardless of label order.

For some  $i \in \{1, \dots, N\}$ , and an indexing set  $J = \{j_1, j_2, \dots, j_M\} \subset \{1, \dots, N\}$ , we seek to minimize  $T_{i,J} = (\sum_{m=1}^M \Delta_{ij_m} p_{ij_m})^2$ . As in our earlier argument we assume no two labels in the neighbor

<sup>1</sup>[https://pytorch.org/hub/pytorch\\_vision\\_resnet/](https://pytorch.org/hub/pytorch_vision_resnet/)

<sup>2</sup>[https://huggingface.co/docs/transformers/en/model\\_doc/distilbert](https://huggingface.co/docs/transformers/en/model_doc/distilbert)

<sup>3</sup><https://docs.pytorch.org/vision/main/models/efficientnet.html>

<sup>4</sup><https://huggingface.co/facebook/hubert-base-ls960>

<sup>5</sup><https://pypi.org/project/noisereduce>

<sup>6</sup><https://huggingface.co/openai/whisper-tiny>

<sup>7</sup><https://huggingface.co/google-bert/bert-base-uncased>

<sup>8</sup>[https://machinehack.com/hackathons/predict\\_the\\_price\\_of\\_books/overview](https://machinehack.com/hackathons/predict_the_price_of_books/overview)

<sup>9</sup><https://www.kaggle.com/datasets/ericpierce/austinhousingprices>

set being considered are equal, and, without loss of generality, if  $m_1 < m_2$ , then  $y_{j_{m_1}} < y_{j_{m_2}}$ . Additionally, no labels in the neighbor set are equal to  $y_i$ . If  $R = \sum_{m=1}^M p_{ij_m}$  as before, then this is a convex quadratic optimization with respect to the vector  $p_i^* = (p_{ij_1}, \dots, p_{ij_M})$  over the standard simplex scaled by  $R$ . Let  $\{e_1, \dots, e_M\}$  be the standard basis vectors in  $\mathbb{R}^M$  and define  $\lambda = \frac{\Delta_{ij_{m+1}}}{\Delta_{ij_{m+1}} - \Delta_{ij_m}}$ . Immediately, we see that there is a solution to our optimization given by the vector

$$p_i^* = \begin{cases} R \cdot e_1, & y_i < y_{j_1} \\ R \cdot e_M, & y_i > y_{j_M} \\ \lambda R \cdot e_m + (1 - \lambda) R \cdot e_{m+1}, & y_{j_m} < y_i < y_{j_{m+1}}, \text{ for some } 1 < m < M \end{cases}$$

The case of interest, where a nontrivial optimal structuring condition may be found, is the final one. However, this case yields the same triplet condition as in the original argument. This proves that an additional condition for higher order structures is not guaranteed by a partial optimization of  $T_{iJ}$ . While this argument does not preclude the possibility of higher order structuring, further insight is needed to uncover such conditions.